NANO LETTERS

Letter

pubs.acs.org/NanoLett

Efficient, Uniform, and Large Area Microwave Magnetic Coupling to NV Centers in Diamond Using Double Split-Ring Resonators

Khadijeh Bayat,*[,†] Jennifer Choy,[†] Mahdi Farrokh Baroughi,[‡] Srujan Meesala,[†] and Marko Loncar[†]

[†]School of Engineering and Applied Sciences, Harvard University, Cambridge, Massachusetts 02138, United States

[‡]Department of Electrical Engineering and Computer Science, South Dakota State University, Brookings, South Dakota 57007, United States

ABSTRACT: We report on the development and utilization of a double split-ring microwave resonator for uniform and efficient coupling of microwave magnetic field into nitrogen-vacancy (NV) centers in a diamond over a mm^2 area. Uniformity and magnitude of delivered microwave field were measured using the Rabi nutation experiment on arrays of diamond nanowires with ensemble NV centers. An average Rabi nutation frequency of 15.65 MHz was measured over an area of 0.95 × 1.2 mm, for an input microwave power of 0.5 W. By mapping the Rabi nutation frequency to the magnetic field, the average value of the magnetic field over the aforementioned area and input microwave power was 5.59 G with a standard division of 0.24 G.

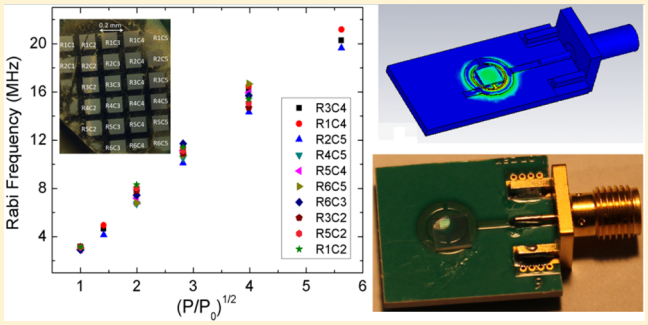

KEYWORDS: *Diamond, nitrogen vacancy, spintronics, electron spin resonance, magnetic resonance, microwave resonator*

The negatively charged nitrogen-vacancy (NV) center is an attractive platform for magnetic sensing.[1−3] Due to the small size of the NV center, it can be implanted within few nanometers from the surface of the diamond and thus within few nanometers away from the magnetic sample, allowing for magnetic sensing with nanoscale resolution. Moreover, an NV-based magnetic sensor works under ambient conditions and is biocompatible, which makes it a great candidate for bioimaging.[4]

To coherently manipulate the spin state of NV for magnetic sensing, electromagnetic field at the frequencies near to that of electron spin resonance (ESR) is applied. For bulk magnetometry applications[5,6] it is beneficial to excite large ensemble of NV centers at the same time since the minimum magnetic field that can be detected is proportional to $1/\sqrt{N}$, where N is the total number of the probed NVs.[1] Theoretical estimates predict that a magnetic sensor based on NV ensembles with NV densities of $\approx 10^{15}-10^{17}$ cm^{-3} distributed throughout the volume of mm^3 diamond sample would result in an ultrahigh sensitivity at $fT/(Hz)^{1/2}$ scales.[1,7] For this to work, however, uniform magnetic fields over the whole sample volume are needed. Unfortunately, conventional microwave delivery techniques based on a copper wire, loop antenna, or coplanar waveguide[8−10] can only address NV centers within a small range, for example, ∼30 and ∼150 μm in the case of wire [8] and loop antenna,[9] respectively. To overcome this limitation, we have developed double split-ring microwave resonators which can address NV centers over a mm^3 volume. Moreover, our approach increases the efficiency of microwave delivery and increases the strength of NV−microwave interaction by more than 8-fold.

Figure 1a shows the picture of the fabricated double split-ring resonator on the printed circuit board (PCB). The double split-ring resonator[11,12] is formed by two magnetically coupled transmission lines terminated by two gaps as shown in Figure 1a. The microwave power is supplied via a 50 Ω microstrip line which is coupled to the double split-ring resonator through a capacitive gap which serves as the impedance matching element.

Figure 1b shows the simulated distribution of the normal component of the magnetic field at the frequency of 2.87 GHz on the surface of a 3 × 3 × 0.5 mm diamond sample mounted on the resonator. The field distribution is fairly uniform over a 1 mm^2 area of the diamond.

The NV center is a point defect in diamond, which consists of a substitutional nitrogen neighboring a vacant lattice point. Negatively charged NV has an extra electron at the defect site resulting in paramagnetic properties. Due to the crystal field, the spin levels are split by 2.87 GHz, shown in Figure 2a, with $m_s = 0$ in the lowest energy level and the $m_s = \pm 1$ in the highest energy level. Spin polarization and readout are carried out by green (532 nm) excitation and red (637−800 nm) fluorescence detection.[5] An external magnetic field lifts the degeneracy of $|\pm 1\rangle$ state with a Zeeman shift given by $\Delta = m_s \gamma B_{\parallel}$, where γ and $B_{\parallel}$ are the NV gyromagnetic ratio $\gamma = g\mu_B/h$

Received: November 1, 2013
Revised: February 14, 2014
Published: February 26, 2014

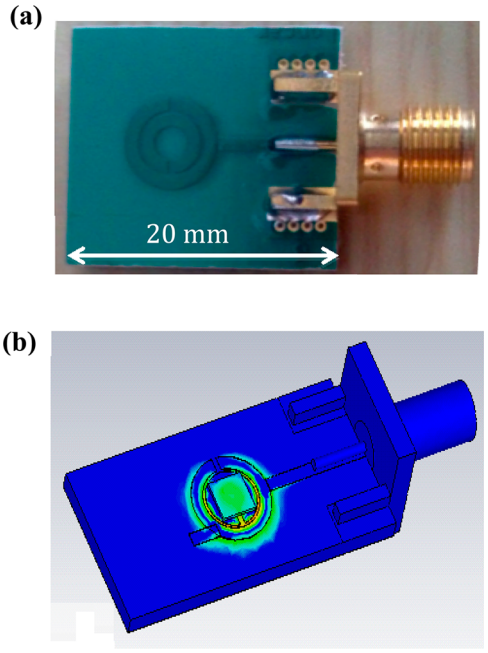

Figure 1. (a) Fabricated double split-ring resonator on a PCB. (b) Distribution of the normal component of magnetic field intensity in a diamond loaded resonator in logarithmic scale. The outline of the copper stub used to tune the resonance frequency of the resonator can be seen as a rectangle close to the bottom left edge of the diamond.

= 2.8MHz/G and projection of magnetic field along the NV symmetry axis, respectively.[2] Thus, the NV's ESR frequency shifts in the presence of the external magnetic field.

An initial design of our microwave resonator was based on the analytical formulation proposed by Shamonin et al. [13] and was then refined using full-wave numerical simulations (CST Microwave Studio V. 2012.08). The design parameters are depicted in the 2D sketch of the resonator shown in Figure 2c. The magnitude of S_{11}, known as the return loss of the resonator, highly depends on the size of the coupling gap (g_c). In order to minimize the return loss and maximize the microwave power coupled to the resonator, the gap size should be as small as possible. In our case, the optimized gap size was found to be 50 μm. The ratio between the electromagnetic energy stored in the resonator and the energy lost in one cycle, quality factor (Q), is inversely proportional to the sum of the ohmic loss in metal wires, the dielectric loss of the printed circuit board (Rogers 6010.2L substrate), radiation loss, and coupling loss of the microstrip line. A large Q results in a large magnetic field intensity at the center of the resonator, at the expense of the reduced bandwidth (BW) and response time of the resonator. Therefore, the optimized resonator design would have low-Q and be critically coupled to the feeding strip line. Table 1 lists the geometrical dimensions of the resonator optimized for a very low S_{11} of approximately −25 dB, Q factor of ∼120, and resonance frequency around 2.974 GHz. Figure 2b shows simulated S_{11} response of the SRR before and after placing a single crystal diamond sample (dimensions 3 × 3 × 0.5 mm) at the middle of the resonator. It can be seen that diamond results in a red shift of the resonance frequency of ∼110 MHz, without affecting the quality factor (Figure 2b). The frequency shift is attributed to the changes in the effective dielectric constant of the resonator due to the presence of diamond.

As illustrated by Figure 1b the distribution of the normal component of the magnetic field intensity at the top surface of the diamond is fairly uniform, with an average of H_z = 354.8 A/m, average B_z = 4.46 G, for an input power of P_{in} = 1 W. The variation of H_z along x, y, and z directions over 1.5 × 1.5 mm area and thickness of 0.5 mm is less than 6.5%, 10%, and 1%, respectively. The stored electromagnetic energy in the resonator can be found as $(1 - S_{11}^2)QP_{in}/\omega_r$, where P_{in} represents the input microwave power delivered to the device and ω_r represents the resonance frequency of the resonator. As a consequence, the magnitude of the magnetic field intensity at any point with coordinates (x,y,z) inside the resonator can be given by $C(x,y,z)((1 - S_{11}^2)QP_{in}/\omega_r)^{1/2}$. $C(x,y,z)$ takes into account spatial distribution of the field, and also depends on the geometry and material composition of the resonator. In our case, given the uniform field distribution, we can use approximation $C(x,y,z) \approx C(x_c,y_c,z_{PCB})$, that is the value at the center of the resonator at PCB/diamond interface. Based on the simulation of Figure 1b, we get $C(x_c,y_c,z_{PCB})$ = 5.48 × 10^4 G/$\sqrt{\text{J}}$. This can be used to make estimates of the magnetic field for a given input microwave power.

The resonance frequency of the resonator can be tuned over a wide range by controlling its inner radius r_1 (please see the inset of Figure 2c). To confirm this experimentally, 10 devices, with different inner radius, were fabricated by Sierra Company and characterized by a Network Analyzer. Figure 2c is a plot of the resonance frequency of fabricated resonators (blue markers) as a function of r_1. The test results show that by changing r_1 from 1 to 1.3 mm, the resonant frequency can be varied between 2.6 and 2.97 GHz. Moreover, the resonance frequency is linearly dependent on inner radius of the resonator with a slope of −1.153 GHz/mm.

Figure 2d shows the experimental S_{11} response of a resonator with r_1 = 1 mm and r_2 = 2.2 mm in the frequency range of 2.75−3.00 GHz. We find resonance frequency of f = 2.974 GHz, $S_{11} \sim -35$ dB, Q = 72 and BW = 40 MHz. Using these parameters, we estimate that 99.97% of the input power at center resonance frequency directly couples to the resonator and contributes to the enhanced stored electromagnetic field in the system. The S_{11} spectrum of loaded resonator, after placing a diamond sample with dimensions of 3 × 3 × 0.5 mm^3 on top of it, reveals the resonance frequency f = 2.874 GHz, $S_{11} \sim -25$ dB, Q = 70, and BW = 40 MHz (Figure 2d). A red shift in the resonance frequency of 100 MHz is in good agreement with simulation results shown in Figure 2b.

In order to use the microwave resonator for optically detected magnetic resonance applications, it is important to be able to tune its resonance frequency to the NV's ESR frequency. This fine-tuning can be achieved by a strip of copper tape placed close to the outer ring of the resonator (Figure 1b), without affecting Q significantly. The use of stubs and strips for frequency tuning is common practice in microwave circuitry.[14] In our case, the copper tape affects the capacitive coupling between the outer ring and the ground plane (backside of the PCB) and hence shifts the resonance frequency. We found in our resonator configuration that a copper tape of 1.5 × 1.5 mm^2 in size can tune the resonance frequency within a 400 MHz window depending upon the positioning of the tape. For fine-tuning, the microwave resonator is connected to the Agilent Network Analyzer, and the size and location of the copper tape is varied to achieve the desired center frequency. Using this approach, we were able to shift the resonant frequency from 2.874 GHz (Figure 2d) to

dx.doi.org/10.1021/nl404072s | Nano Lett. 2014, 14, 1208−1213

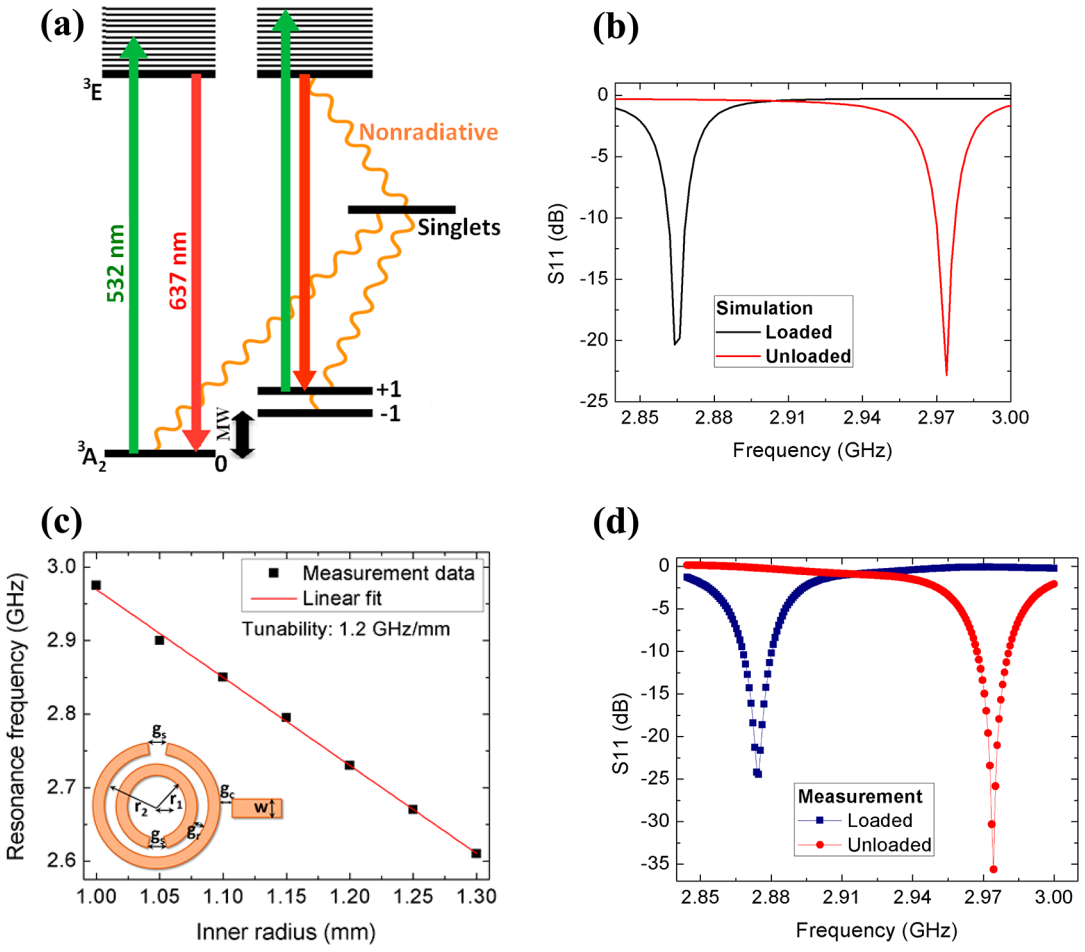

Figure 2. (a) Energy band diagram of a negatively charged NV center. Electronic spin readout is carried out by 532 nm excitation and red (638−800 nm) fluorescence detection. Spin manipulation in ground-state triplet is performed by applying MW power at ∼2.87 GHz, zero magnetic field splitting. (b) Simulated S_{11} spectrum of the resonator without (red) and with (blue) diamond sample introduced. The geometrical parameters listed in Table 1 were obtained from these simulations, where r_1 and r_2 are 1.2 and 2.4 mm, respectively. (c) Measured resonance frequency of the microwave resonator as a function of the radius of the inner ring along with the 2D sketch of the resonator, where r_1 and r_2 are the radii of the inner and outer rings and g_c, g_s, and g_r are the coupling gap, gap at the split, and the gap between the two rings, respectively. (d) Measured S_{11} spectrum of loaded (with diamond) and unloaded (without diamond) resonator. A single crystal electronic grade diamond sample, with the dimensions of 3 × 3 × 0.5 mm, was used in these experiments. The radii of inner and outer rings are r_1 = 1 mm and r_2 = 2.2 mm, respectively.

Table 1. Geometrical Dimensions of a Resonator with Quality Factor of Q = 120 with a Resonance Frequency of 2.974 GHz[a]

parameter	value	parameter	value
ε_r	10.2	w	1 mm
t_{Cu}	9 μm	g_c	0.05 mm
tan(δ)	0.0023	g_r	0.2 mm
r_1	1.2 mm	g_s	0.4 mm
r_2	2.4 mm		

[a] ε_r, t_{Cu}, tan(δ), r_1, r_2, w, g_c, g_r, and g_s are dielectric constant of the board, thickness of the copper layer on the board, loss tangent of the board material, inner radius, outer radius, coupling gap, gap between the rings, and gap size at the split of each ring, respectively; please refer to Figure 2c.

2.87 GHz (ESR resonance of NV) and perform further characterization of the system, as discussed below.

To better visualize the uniformity of the magnetic microwave field over a mm^2, ESR measurements were performed (in ambient conditions) on NV ensembles implanted inside diamond nanowires. The characterization setup, based on a home-built confocal microscope with a long working distance objective (4 mm) and numerical aperture of 0.6, is illustrated in Figure 3a. To fabricate the samples, electronic grade diamond substrates (Element 6) were first cleaned in a boiling mixture of nitric, sulfuric, and perchloric acids. Diamond nanowires were then made on these substrates using electron beam lithography followed by reactive ion etching processes.[15] The samples were then cleaned using the aforementioned boiling process. The sidewalls of the nanowires were implanted by nitrogen ions at a dosage of 10^{13} cm^{-2} and energy of 35 keV in a −45° incident ion angle with respect to the x−y plane. The implantation process was conducted from 4 sides at 90° rotational steps. A rapid thermal anneal at 1000 °C for 1 min was conducted in nitrogen to treat the crystallographic defects induced by ion implantation process and form and activate the negatively charged nitrogen vacancy ensembles. Figure 3b shows the optical image of the diamond sample with 5 × 6 array of nanowire patches, each having an area of 150 × 150 μm and patch-to-patch separation of 50 μm. The total area of the probed region is 0.95 × 1.2 mm. The thickness of the diamond substrate is 0.5 mm. Figure 3c shows the SEM image of the fabricated nanowires imaged at a 30° tilt. The radius and height

dx.doi.org/10.1021/nl404072s | Nano Lett. 2014, 14, 1208−1213

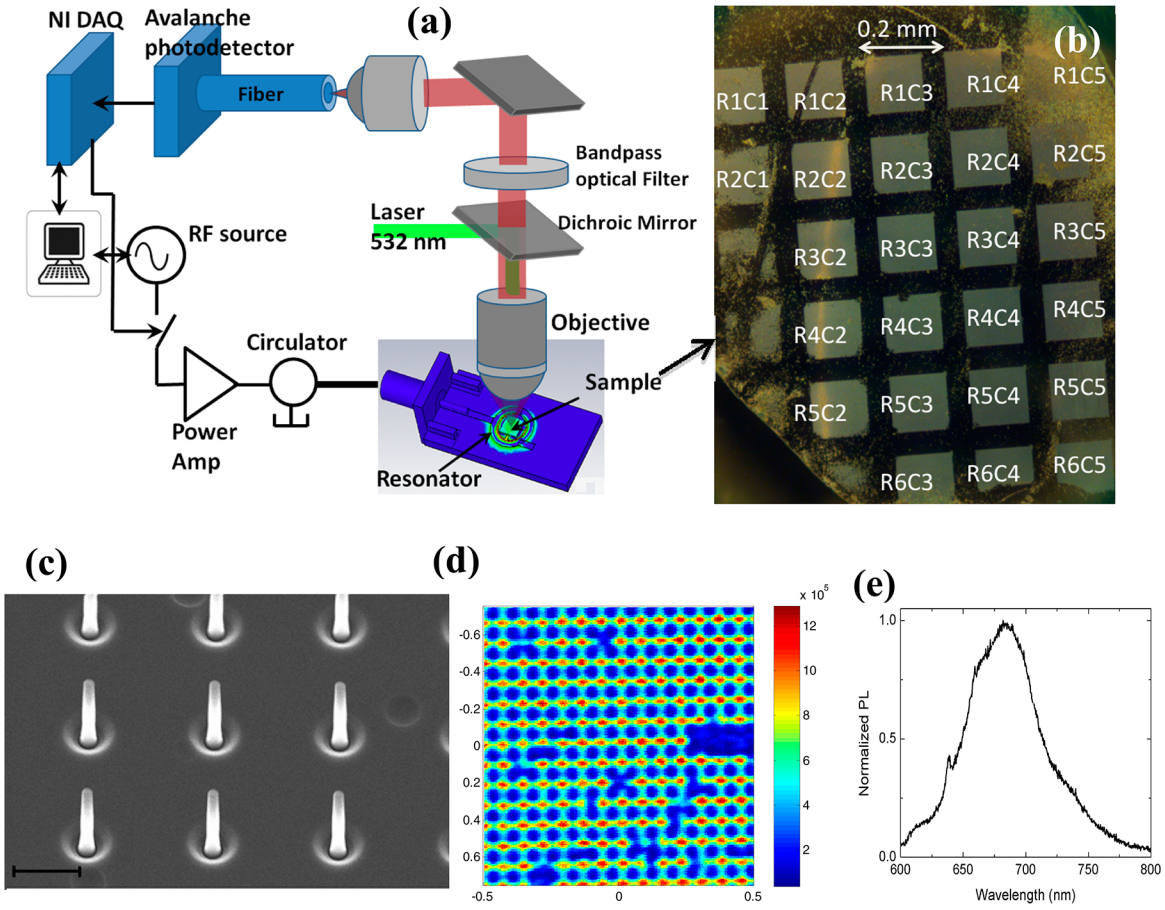

Figure 3. (a) Schematics of the measurement setup consisting of a scanning confocal microscope equipped with a microwave power delivery circuitry, and an avalanche photodetector. (b) Optical image of the nanowire array sample used for the measurements. The dimension of each nanowire patch is 150 × 150 μm with a spacing of 50 μm with a total area of 0.95 × 1.2 mm. (c) SEM image of the nanowires with diameter, height, and spacing of 250 nm and 2 and 2 μm, respectively. The scale bar depicted in the figure is 1 μm. (d) The confocal PL image of a nanowire array for laser power of 0.6 mW measured using the home-built confocal microscope shown in (a). (e) A typical PL spectrum of nanowire with ensemble NV with zero-phonon line at 637 nm and phonon sideband in the 640−780 nm wavelength window.

of each nanowire and the spacing between them are approximately 250 nm and 2 and 2 μm, respectively. Figure 3d shows the measured fluorescence image of a typical nanowire array. A uniform distribution of fluorescent diamond nanowires is observed. Photon count reaches to over a million counts per second (CPS) under an excitation power of 0.6 mW. Under similar measurement conditions, count rates from a single NV inside a nanowire (data not shown) are between 50 000 and 55 000 CPS. Therefore, we conclude that the photoluminescence signal is being detected from ∼20 NV centers on average. Finally, Figure 3e shows the photoluminescence spectra of photons collected from a typical nanowire with ensemble NV, featuring characteristic zero-phonon line peak of NVs around 637 nm and phonon sideband spectra ranging from 640 to 780 nm.

Figure 4a shows a typical ESR spectrum of a nanowire for an input microwave power of 30 mW. This is a signature ESR spectrum of nitrogen vacancy with a minimum photoluminescence at 2.87 GHz and a contrast of 10% confirming the formation of NV centers in diamond nanowires. The spectrum of the coupled power into the resonator utilized for conducting the ESR measurements, $1 - S_{11}^2$, is also included in the figure, blue curve. The full width half minima (fwhm) of the ESR spectrum is 14 MHz, for which more than 95% of the input microwave power is coupled to the resonator. We note that Q of this resonator has dropped to 40 (BW ∼ 71 MHz), which is due the glue used for securing the diamond sample. A small Q and large bandwidth results in a short microwave photon storage/loading time (lifetime) of $\tau = Q/(2\pi f) \sim 2.2$ ns, which makes our approach suitable for fast pulsed ESR applications, as well.

The Rabi nutation frequencies were measured on the labeled nanowire patches (R_1C_1−R_6C_5). A typical Rabi curve for an input microwave power of 1 mW before the amplifier is shown in Figure 4b. Considering the 30 dB gain of the amplifier and the −3 dB loss of the microwave switch and isolator, the actual power fed to the resonator is 0.5 W resulting in the Rabi nutation frequency of 16.69 MHz. This is nearly an order of magnitude larger than frequencies (∼1.8 MHz) typically achieved using loop antenna or a copper wire for microwave delivery, for the same input power. The component of magnetic field perpendicular to the NV symmetry axis, $\mathbf{B}_1$, can be calculated from the Rabi nutation frequency, Ω, using the following equation:

$$\Omega = \gamma \mathbf{B}_1 \tag{1}$$

The measured values of Rabi nutation frequency and $\mathbf{B}_1$ for different nanowire patches, listed in Table 2, are fairly uniform over the entire measurement area (0.95 × 1.2 mm): Rabi frequency is in the range of 14.34−16.69 MHz (standard

dx.doi.org/10.1021/nl404072s | Nano Lett. 2014, 14, 1208−1213

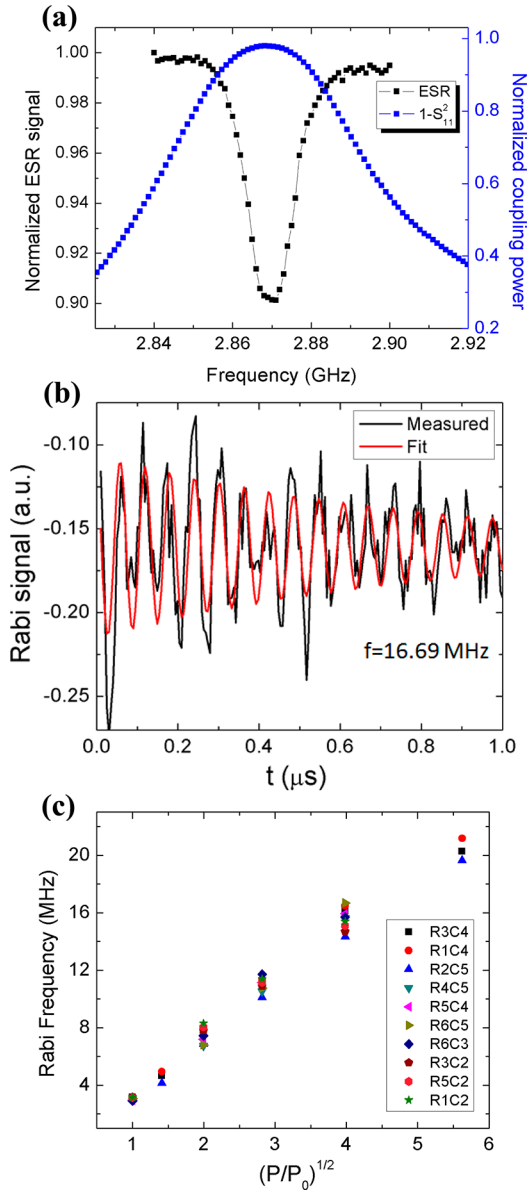

Figure 4. (a) A typical ESR spectrum of a nanowire with a dip at 2.87 GHz, fwhm of 14 MHz, and contrast of about 11% measured using 30 mW incident microwave power (black curve). Normalized power coupled into the resonator ($1 - S_{11}^2$) is also shown (blue curve). The fwhm of the ESR signal is about 14 MHz. More than 95% of the incident power is coupled to the resonator within the width of half minimum of the ESR spectrum. The BW of the resonator is about 71 MHz. (b) A typical Rabi signal obtained from a diamond nanowire in Figure 3b measured for an incident microwave power of 500 mW. This results in a 16.69 MHz Rabi nutation frequency. (c) A plot of Rabi nutation frequency versus normalized microwave power $(P/P_0)^{1/2}$, where P and P_0 are the input microwave power and 31.6 mW (minimum input power) at different nanowire patches labeled in Figure 3b.

deviation of 0.68 MHz and normalized standard deviation of 4.4%), while $\mathbf{B}_1$ is in the range of 5.13−5.96 G (standard deviation of 0.24 G and normalized standard deviation of 4.4%). This confirms that the microwave resonator delivers a uniform magnetic field over a mm^2 area scale, as predicted by full wave numerical analysis. Finally, Figure 4c shows the Rabi nutation frequency versus square root of the normalized microwave input power, $(P/P_0)^{1/2}$, where P_0 is 31.6 mW, for

Table 2. Distribution of the Rabi Nutation Frequency and $\mathbf{B}_1$ for Different Nanowire Sets Marked in Figure 3b and Their Statistical analysis

nanowire set	Rabi nutation frequency (MHz)	$\mathbf{B}_1$ (G)
R1C2	15.40	5.5
R1C4	16.46	5.88
R2C3	15.90	5.68
R2C5	14.34	5.12
R3C2	14.70	5.25
R3C4	16.10	5.75
R4C3	15.88	5.67
R4C5	15.62	5.58
R5C4	15.09	5.39
R5C2	15.93	5.69
R6C3	15.71	5.61
R6C5	16.69	5.96
mean	15.65	5.59
standard deviation	0.68	0.24
(STD/mean)%	4.4	4.4

labeled nanowire patches. It can be seen that the Rabi nutation frequency has a linear relationship with $(P/P_0)^{1/2}$ and that its variation for different areas of the nanowire sample is very small.

In summary, a double split-ring microwave resonator was utilized for uniform and efficient coupling of microwave magnetic field into nitrogen vacancy centers in diamond over an area of mm^2. To map the microwave magnetic field distribution and strength of the microwave resonator, the Rabi nutation experiment was performed on an NV ensemble diamond nanowire sample with an area of 0.95 × 1.2 mm. More than 8-fold enhancement in microwave field coupling to NV center in comparison to that a loop antenna and copper wire was observed over 50× larger area. Moreover, highly uniform microwave magnetic field distribution with <5% normalized standard deviation over the aforementioned area was achieved. Based on these results, we conclude that microwave resonator approach using split ring structure is advantageous over the loop antenna and copper wire approaches for delivering microwave signal to NV centers in diamond as it provides uniform and strong magnetic field over rather large area. Furthermore, this method is much more energy efficient as it couples majority of the input power to the resonator. We hope that our approach will find widespread application in NV-center based room-temperature precision magnetometry and bioimaging.

AUTHOR INFORMATION

Corresponding Author

*E-mail: kbayat@seas.harvard.edu.

Notes

The authors declare no competing financial interest.

ACKNOWLEDGMENTS

The diamond devices were fabricated at the Center for Nanoscale Systems at Harvard University. K.B. would like to thank NSERC Canada for its support. Also, authors would like to thank R. Walsworth, C. Belthangady, L. Pham, I. Bulu, A. Kabiri, and M. Grinolds for fruitful discussions and suggestions. This work was supported in part by the Defense Advanced Research Projects Agency (QuASAR program) as well as by grant from Schlumberger-Doll research center.

REFERENCES

(1) Taylor, J. M.; Cappellaro, P.; Childress, L.; Jiang, L.; Budker, D.; Hemmer, P. R.; Yacoby, A.; Walsworth, R.; Lukin, M. D. High-sensitivity diamond magnetometer with nanoscale resolution. *Nat. Phys.* **2008**, *4*, 810−816.

(2) Maze, J. R.; Stanwix, P. L.; Hodges, J. S.; Hong, S.; Taylor, J. M.; Cappellaro, P.; Jiang, L.; Dutt, M. V. G; Togan, E.; Zibrov, A. S.; Yacoby, A.; Walsworth, R. L.; Lukin, M. D. Nanoscale magnetic sensing with an individual electronic spin in diamond. *Nature* **2008**, *455*, 644−647.

(3) Degen, C. L. scanning magnetic field microscope with a diamond single-spin sensor. *Appl. Phys. Lett.* **2008**, *92*, 243111.

(4) Le Sage, D.; Arai, K.; Glenn, D. R.; DeVience, S. G.; Pham, L. M.; Rahn-Lee, L.; Lukin, M. D.; Yacoby, A.; Komeili, A.; Walsworth, R. L. Optical magnetic imaging of living cells. *Nature* **2013**, *496*, 486−489.

(5) Hong, S.; Grinolds, M. S.; Pham, L. M.; Le Sage, D.; Luan, L.; Walsworth, R. L.; Yacoby, A. Nanoscale magnetometry with NV centers in diamond. *Mater. Res. Soc. Bulletin* **2013**, *38*, 155−161.

(6) Pham, L. M.; Le Sage, D.; Stanwix, P. L.; Yeung, T. K.; Glenn, D.; Trifonov, A.; Cappellaro, P.; Hemmer, P. R.; Lukin, M. D.; Park, H.; Yacoby, A.; Walsworth, R. L. Magnetic field imaging with nitrogen-vacancy ensembles. *New J. Phys.* **2011**, *13*, 045021.

(7) Acosta, V. M.; Bauch, E.; Ledbetter, M. P.; Santori, C.; Fu, K. M. C.; Barlay, P. E.; Beausoleil, R. G.; Linget, H.; Roch, J. F.; Tressart, F.; Chemersov, S.; Gawlik, W.; Budker, D. Diamonds with a high density of nitrogen-vacancy centers for magnetometry applications. *Phys. Rev. B.* **2009**, *80*, 115202.

(8) Lai, N. D.; Zheng, D.; Jelezko, F.; Treussart, F.; Roch, J. F. Influence of a static magnetic field on the photoluminescence of an ensemble of nitrogen-vacancy color centers in a diamond single-crystal. *Appl. Phys. Lett.* **2009**, *95*, 133101.

(9) Stanwix, P. L.; Pham, L. M.; Maze, J. R.; Le Sage, D.; Yeung, T. K.; Cappellaro, P.; Hemmer, P. R.; Yacoby, A.; Lukin, M. D.; Walsworth, R. L. Coherence of nitrogen-vacancy electronic spin ensembles in diamond. *Phys. Rev. B* **2010**, *82*, 201201.

(10) De Lange, G.; Van Der Sar, T.; Block, M.; Wang, Z-H.; Dobrovitsi, V.; Hanson, R. Controlling the quantum dynamcis of a mesoscopic spin bath in diamond. *Sci. Rep.* **2012**, *2*, 382.

(11) Gil, M.; Aznar, F.; Velez, A.; Duran-Sindreu, M.; Selga, J.; Siso, G.; Bonache, J.; Martin, F. In *Passive microwave components and Antennas*; Zhurbenko, V., Ed.; Intech: Rijeka, Croatia, 2010; Chpt 9

(12) Aydin, K.; Cakmak, A. O.; Sahin, L.; Li, Z.; Bilotti, F.; Vegni, L.; Ozbay, E. Split-ring-resonator-coupled enhanced transmission through a single subwavelength aperture. *Phys. Rev. Lett.* **2009**, *102*, 013904.

(13) Shamonin, M.; Shamonina, E.; Kalinin, V.; Solymar, L. Resonant frequencies of a split-ring resonator: Analytical solutions and numerical simulations. *Microwave Opt. Technol. Lett.* **2005**, *44*, 133−136.

(14) Fehsenfeld, F. C.; Evenson, K. M.; Broida, H. P. Microwave discharge cavities at 2450 MHz. *Rev. Sci. Instrum.* **1965**, *36*, 294−298.

(15) Hausmann, B. M.; Khan, M.; Babinec, T. M.; Zhang, Y.; Martinick, K.; McCutcheon, M. W.; Hemmer, P. R.; Lončar, M. Fabrication of diamond nanowires for quantum information processing applications. *Diamond Relat. Mater.* **2010**, *19*, 621−629.